Journal of Computational Physics **173,** 549–574 (2001)
doi:10.1006/jcph.2001.6893, available online at http://www.idealibrary.com on IDEAL®

An Efficient High-Order Taylor Weak Statement Formulation for the Navier–Stokes Equations

A. Kolesnikov* and A. J. Baker†

**Flow Sciences, Inc., Wilmington, North Carolina 28401; and †Department of Mechanical and Aerospace Engineering and Engineering Science, The University of Tennessee, Knoxville, Tennessee 37996*
E-mail: akolesnikov@flowsciences.com

Received July 27, 2000; revised July 11, 2001

Traditionally, finite element methods generate progressively higher order accurate solutions by use of higher degree trial space bases for the weak statement construction. This invariably yields matrix equations of greater bandwidth thus increasing implementational and computational costs. A new approach to designing high order, defined here to exceed a third-order accurate method, has been developed and tested. The systematic construction of progressively higher order spatial approximations is achieved via a modified equation analysis, which allows one to clearly identify appended terms appropriate for a desired accuracy order. The resulting "modified" PDE is shown to be consistent with the Taylor Weak Statement (TWS) formulation. It confirms the expected high order of spatial accuracy in TWS constructions and provides a highly efficient dispersion error control mechanism whose application is based on the specifics of the solution domain discretization and physics of the problem. A distinguishing desirable property of the developed method is solution matrix bandwidth containment, i.e., bandwidth always remains equal to that of the linear basis (second-order) discretization. This permits combining the computational efficiency of the lower order methods with superior accuracy inherent in higher order approximations.

INTRODUCTION

Higher order methods can generate very accurate results for problems with smooth data, that is, solutions for which the physical domain is smoothly mapped onto the computational space. This is accomplished by increasing the degree of the trial space basis [27], which invariably yields matrix equations of greater bandwidth. This increases the implementational cost, but by lowering the truncation error can reduce the number of nodes needed to obtain a given accuracy numerical solution for smooth data.

Finite difference methods approximate partial derivative entries of a given PDE on an individual basis. The value of each derivative at a generic computational node is

0021-9991/01 $35.00

approximated by a linear combination of function values at the adjacent nodes. Consequently, coefficients of this combination are established by matching Taylor series coefficients [34].

Using additional nodes for wider computational stencil permits a higher order accuracy by introducing more unknowns into the approximation expression. Generalization of this approach is provided by Pade or by compact finite difference schemes [22, 25].

Alternatively, a higher order approximation for select elliptic problem statements can be achieved using Hermitian type discretization methods [9] without adding additional pivotal points. In this case, nodal values of higher order derivatives are used to introduce more coefficients in the stencil expressions, e.g.,

$$a_1 Q_{j-1} + a_2 Q_j + a_3 Q_{j+1} + a_4 Q''_{j-1} + a_5 Q''_j + a_6 Q''_{j+1} = 0. \tag{1}$$

Once stencil coefficients are determined by Taylor series analysis, solution matrix bandwidth expansion is contained by expressing high-order derivatives via nodal function values.

Unless this transition can be enabled by the partial differential equation itself, the solution matrix bandwidth must be expanded to accommodate the extra unknowns resulting from introducing nodal values of higher order derivatives into the stencil expression. Here again, a higher order approximation comes at a computational price of solving matrix equations of greater bandwidth. Of particular importance, this is clearly the case for the advection–diffusion equation, which does not provide a dependence between derivatives and corresponding function values, rendering Hermitian methods ineffective in reducing computational cost.

Approximation can be further optimized by introducing additional theoretical considerations, suitable for a particular physical problem. Optimized compact finite difference schemes [19, 33, 35] utilize Fourier analysis to achieve maximum resolution by minimizing dispersive (phase) errors in the differencing approximation. Resolution of sharp boundary layers in convection dominated problems, and shock-like discontinuities caused by local nonlinearities, can be enhanced by promoting the scheme's "monotonicity."

Thus, the analysis of a normalized-variable diagram leads to the restrictions being placed on time-averaged normalized face values of the solution resulting in the ULTIMATE strategy [24] for modulating a numerical solution, which can be applied for arbitrarily high-order schemes. Similarly, comparison of relevant divided differences to select the locally smoothest stencil, as used on the reconstruction stage of the interpolation procedure described by Shu [32] for ENO and WENO type schemes, yields highly accurate solutions.

Finite element methods proceed in a fundamentally different manner. The cornerstone of the theoretical development is the "weak form" formulation [3] requiring the measure of the error in the approximate solution to vanish in an integrated sense. Introduction of the solution domain discretization further replaces the continuous solution approximation with its appropriate piecewise-continuous form, resulting in generation of the "weak statement" extremum, a precise definition of the computational stencil expressions upon specification of suitable test and trial basis function sets.

A higher order of approximation is achieved by general or local embedding of higher degree interpolants (p-refinement, see [27]). Method performance can be enhanced by "optimizing" test basis function sets leading to various Petrov–Galerkin approximations [5, 6].

Optimal $h - p$ finite element methods [27] use bilinear form symmetrization to derive problem specific test and trial functions. The existence of an accurate fine mesh solution to a given problem is assumed, and the corresponding optimal test and trial functions are designed to match this solution at the nodes of a significantly coarser grid. This leads to the "extrasuperconvergence" result which allows for an *a posteriori* error estimate on each of the finite elements of the solution domain discretization, yielding an adaptive mesh refinement strategy.

Early Petrov–Galerkin methods [8, 13] introduced excessive amounts of diffusion into the numerical solution, and SUPG methods [5] were designed to counter this problem. Extension of the Lax–Wendroff method [23], which uses the governing equation to cancel error terms in time and space to a finite element formulation, led to development of the Taylor–Galerkin method of Donea [10], which was generalized as the Taylor weak statement (TWS) by Baker and Kim [2]. Detailed investigation of the TWS method performance for various multidimensional problems can be found in [6, 7].

Matrix/static condensation techniques, unique for finite element formulations, provide another powerful tool for method optimization. The SGM method of Roy and Baker [28, 29], and Galerkin methods with bubble functions [1], successfully use this approach to promote solution stability and monotonicity. Finite element methods specifically designed for shock-capturing were shown to significantly improve the method's ability to resolve sharp solution discontinuities. Examples include discontinuous Galerkin methods [14] and a nonlinear element–upstream weak statement (NEWS) algorithm [16, 17], that achieves accurate monotone solutions for various conservation law system forms.

Overall, upon discretization of the solution domain, virtually all high-order methods result in matrix equations with larger bandwidths thus increasing the computational cost. Such wider stencils cannot be implemented at the boundaries, leading to a local loss of accuracy, especially in multidimensional cases, hence requiring additional theoretical consideration. Grid generation around complex geometries also becomes extremely complicated, since a smooth grid is dictated by the design of high-order methods.

Recently, a method resolving this dilemma was developed and tested [21]. The theory provides high-order accurate solutions at no added computational cost, by retaining the solution matrix bandwidth of the second-order methods. This is potentially significant in simplifying multidimensional grid generation procedures necessary for the implementation of high-order methods. The development utilizes the ideas of "modified" partial differential equation analysis of Warming and Hyett [36] (see also [31]) to derive the problem-specific computational stencil coefficients appropriate for the desired order of accuracy. This allows for avoiding implementational difficulties encountered by Hermitian type methods.

The systematic construction of progressively higher order spatial approximations is achieved via a modified equation analysis, which allows one to clearly identify correction terms appropriate for a desired accuracy order. The resulting perturbed PDE is shown to be consistent with the Taylor Weak Statement formulation. It confirms the expected high order of spatial accuracy in TWS constructions and provides a highly efficient dispersion error control mechanism whose application is based on the specifics of the solution domain discretization and physics of the problem.

The present paper extends the developed formulation to benchmark problem applications for the Navier–Stokes equations. The paper is organized as follows. It presents the theoretical analysis for nonlinear advection–diffusion problems in one and two dimensions. Numerical simulations compare performance of the developed method to that of the linear and bilinear

basis Galerkin finite element formulations. Uniform mesh refinement convergence results confirm the order of truncation error, correlated with an asymptotic error estimate, for each method. The generated high-order TWS formulation is shown to require significantly fewer nodes to accurately resolve solution gradients for convection dominated problems. Benchmark problem tests for the incompressible Navier–Stokes equations complete the paper.

ONE-DIMENSIONAL STEADY-STATE FORMULATION

Consider the multidimensional advection–diffusion equation with the corresponding Dirichlet and Neumann boundary conditions

$$L(q(\mathbf{x},t)) = \frac{\partial q(\mathbf{x},t)}{\partial t} + \mathbf{f}(\mathbf{x}) \cdot \nabla q(\mathbf{x},t) - \varepsilon \nabla \cdot \nabla q(\mathbf{x},t) = 0 \quad in \quad \Omega \in \mathbf{R}^n \times R^1 \tag{2}$$

$$q = q_b \quad on \quad \partial\Omega_1 \tag{3}$$

$$\frac{\partial q}{\partial \mathbf{n}} = g(\mathbf{x}) \quad \text{on} \quad \partial\Omega_2; \quad \partial\Omega_1 \cup \partial\Omega_2 = \partial\Omega, \tag{4}$$

where viscosity ε and boundary data $g(\mathbf{x})$, q_b are given.

Model equation (2), rewritten for the one-dimensional steady-state case, becomes

$$f(q,x)\frac{dq(x)}{dx} - \varepsilon(x)\frac{d^2q}{dx^2} = 0. \tag{5}$$

Assuming the existence of appropriate boundary conditions, the discrete weak statement formulation is

$$WS^h = S_e([U+D]_e\{Q\}_e) = S_e([A(h,\varepsilon)]_e\{Q\}_e) = \{0\}, \tag{6}$$

where $[U]_e, [D]_e, [A]_e$ are the trial-test function specific matrix forms on the generic FE domain Ω_e.

A fully discrete equivalent of (6), obtained by assembling the element matrix $[A]_e$ on two adjacent elements, yields the generic stencil form

$$f_j(a_1Q_{j-1} + a_2Q_j + a_3Q_{j+1}) - \varepsilon_j(a_4Q_{j-1} + a_5Q_j + a_6Q_{j+1}) = 0 \tag{7}$$

or

$$(f_ja_1 - \varepsilon_ja_4)Q_{j-1} + (f_ja_2 - \varepsilon_ja_5)Q_j + (f_ja_3 - \varepsilon_ja_6)Q_{j+1} = 0. \tag{8}$$

Here, a_i are the coefficients dependent on a specific choice of finite element trial and test functions, and Q_{j-1}, Q_j, Q_{j+1} are the unknown nodal values of the approximate solution. A genuine finite element formulation would require interpolation of functions $f(q,x)$ and $\varepsilon(x)$, thus adding complexity to the stencil expression in (8). In the present analysis, such interpolated functional expressions are replaced with their respective nodal values f_j and ε_j.

Assuming a locally uniform mesh with $\triangle x = h$, which is sufficiently small, and writing a Taylor series expansion at node j yields

$$f_j \left[(a_1 + a_2 + a_3) Q + (a_3 - a_1) h Q_x + (a_3 + a_1) \frac{h^2}{2} Q_{xx} + (a_3 - a_1) \sum_{n=3,2}^{\infty} \frac{h^n}{n!} Q^{(n)} \right.$$
$$\left. + (a_3 + a_1) \sum_{n=4,2}^{\infty} \frac{h^n}{n!} Q^{(n)} \right] - \varepsilon_j \left[(a_4 + a_5 + a_6) Q + (a_6 - a_4) h Q_x \right.$$
$$\left. + (a_6 + a_4) \frac{h^2}{2} Q_{xx} + (a_6 - a_4) \sum_{n=3,2}^{\infty} \frac{h^n}{n!} Q^{(n)} + (a_6 + a_4) \sum_{n=4,2}^{\infty} \frac{h^n}{n!} Q^{(n)} \right] = 0, \tag{9}$$

where Q replaces Q_j for clarity.

Naturally, for (9) to approximate Eq. (5), the a_i in (9) must satisfy the following conditions:

$$\begin{aligned} a_1 + a_2 + a_3 &= 0 \\ a_3 - a_1 &= \frac{1}{h} \\ a_3 + a_1 &= 0 \end{aligned} \tag{10}$$

and

$$\begin{aligned} a_4 + a_5 + a_6 &= 0 \\ a_6 - a_4 &= 0 \\ a_6 + a_4 &= \frac{2}{h^2}. \end{aligned} \tag{11}$$

Coefficient groups $[a_1, a_2, a_3]$ and $[a_4, a_5, a_6]$ are responsible for the second-order discretization of the first- and second-order derivatives, respectively, and conditions (10) and (11) must be satisfied independently of a particular approximation technique selected to arrive at (8). Therefore,

$$\begin{aligned} \frac{\partial q(x)}{\partial x} &= a_1 Q_{j-1} + a_2 Q_j + a_3 Q_{j+1} \\ \frac{\partial^2 q(x)}{\partial x^2} &= a_4 Q_{j-1} + a_5 Q_j + a_6 Q_{j+1}, \end{aligned} \tag{12}$$

and coefficients a_i are uniquely determined by solving (10) and (11),

$$\begin{aligned} a_1 &= -\frac{1}{2h}, \quad a_2 = 0, \quad a_3 = \frac{1}{2h} \\ a_4 &= \frac{1}{h^2}, \quad a_5 = -\frac{2}{h^2}, \quad a_6 = \frac{1}{h^2}. \end{aligned} \tag{13}$$

For the computational stencil coefficients a_i satisfying (13), (9) becomes

$$f_j Q_x - \varepsilon_j Q_{xx} + h^2 \left(\frac{f_j Q_{xxx}}{6} - \frac{\varepsilon_j Q_{xxxx}}{12} \right) + H.O.T. = 0. \tag{14}$$

Rewriting (14) yields the convenient form

$$\varepsilon Q_{xx} = f Q_x + h^2 \left(\frac{f Q_{xxx}}{6} - \frac{\varepsilon Q_{xxxx}}{12} \right) + H.O.T., \tag{15}$$

where f and ε replace f_j and ε_j, respectively.

Equation (15) represents an "infinite" order partial differential equation satisfied by the nodal numerical solution $\{Q\}$ [34, 36]. We therefore can differentiate it repeatedly with respect to x, thus expressing higher order derivatives present in (15), and then attempt to derive a second-order PDE (ODE in the one-dimensional steady-state case), whose second-order approximation would result in a higher order approximation of the equation to be solved. Obtaining this "perturbed" second-order ODE is the key to this theoretical development, since any second-order ODE can be discretized on three nodes in the one-dimensional case.

Assuming for simplicity the viscosity parameter ε is constant, differentiating (15) repeatedly with respect to x and neglecting high-order terms leads to

$$\varepsilon Q_{xxx} = f_x Q_x + f Q_{xx} + H.O.T. \tag{16}$$

$$\varepsilon Q_{xxxx} = f_{xx} Q_x + f_x Q_{xx} + f_x Q_{xx} + f Q_{xxx} + H.O.T. \tag{17}$$

Substituting (16) and (17) into (14) and neglecting the terms of the order greater than 2, one obtains

$$f Q_x - \varepsilon Q_{xx} + h^2 Q_x \left(\frac{f f_x}{12\varepsilon} - \frac{f_{xx}}{12} \right) + h^2 Q_{xx} \left(\frac{f^2}{12\varepsilon} - \frac{f_x}{6} \right) = 0, \tag{18}$$

which represents the equation satisfied by the nodal approximate solution Q and includes the second-order error terms resulting from the selected second-order approximation. Suppose the original equation (5) is now replaced with the following continuous form:

$$f q_x - \varepsilon q_{xx} - h^2 q_x \left(\frac{f f_x}{12\varepsilon} - \frac{f_{xx}}{12} \right) - h^2 q_{xx} \left(\frac{f^2}{12\varepsilon} - \frac{f_x}{6} \right) = 0. \tag{19}$$

The original equation is supplemented here by two correction terms, obtained by reversing the signs on the second-order truncation error contributions in (18). Applying second-order discretization, (12) and (13), to this "perturbed" ODE rather than to the original equation (5) would result in cancellation of the second-order truncation error terms consistent with (18) and therefore provide a fourth-order accurate numerical solution to the original equation. Since only first- and second-order derivatives are present in (19), its second-order discretization does not result in solution matrix bandwidth expansion. The fourth-order accurate numerical solution to the original equation (5) is therefore obtained at no added computational cost as compared to that of the second-order approximation.

It is important to note that for practical applications the viscosity parameter ε is usually small. Hence, for problems with smooth solution and data distributions, it is possible to neglect the terms of the order unity as compared to those of the order $1/\varepsilon$, thus reducing (19) to

$$f q_x - \varepsilon q_{xx} - h^2 q_x \frac{f f_x}{12\varepsilon} - h^2 q_{xx} \frac{f^2}{12\varepsilon} = 0, \tag{20}$$

and combining the terms, the perturbed ODE becomes

$$f\frac{\partial q}{\partial x} - \varepsilon\frac{\partial^2 q}{\partial x^2} - \frac{h^2}{12\varepsilon} f\frac{\partial}{\partial x}\left(f\frac{\partial q}{\partial x}\right) = 0. \tag{21}$$

While numerical solution to (21). would lose its nominal fourth-order of accuracy, it nevertheless could retain the desirable stabilizing effects of high-order approximations. Applicability of this order of magnitude assumption must be carefully evaluated for particular physical problems, since values of function derivatives could be much larger than those of the function itself near points of discontinuity and sharp boundary layers. This assumption is not used in the example advection–diffusion problems considered herein, but its suitability for the Navier–Stokes equation class is discussed later in this paper.

With (19) resulting in a fourth-order accurate solution to the original equation (5), similar development can be shown to yield the following sixth-order perturbed ODE, illustrated for the linear $f(q, x) = u(x)$ case as

$$\begin{aligned} uq_x - \varepsilon q_{xx} - h^2 q_x\left(\frac{uu_x}{12\varepsilon} - \frac{u_{xx}}{12}\right) - h^2 q_{xx}\left(\frac{u^2}{12\varepsilon} - \frac{u_x}{6}\right) - h^4 q_x\left(\frac{uu_x^2}{180\varepsilon^2} - \frac{u^3 u_x}{720\varepsilon^3}\right. \\ \left. - \frac{u_{xxxx}}{360} - \frac{u^2 u_{xx}}{720\varepsilon^2} + \frac{uu_{xxx}}{180\varepsilon}\right) - h^4 q_{xx}\left(\frac{u_{xx}^2}{180\varepsilon} - \frac{u_{xxx}}{90} + \frac{uu_{xx}}{72\varepsilon} + \frac{u^2 u_x}{360\varepsilon^2} - \frac{u^4}{720\varepsilon^3}\right) = 0. \end{aligned} \tag{22}$$

Note, that the terms of the order h^2 remain unchanged from the fourth-order ODE, thus allowing for recursive development of higher order approximations.

First consider a one-dimensional steady-state case for a constant velocity $\mathbf{u}(\mathbf{x}) = u\mathbf{i}$ and Dirichlet boundary conditions. Equation (2) is

$$L(q(x)) = u\frac{dq(x)}{dx} - \varepsilon\frac{d^2 q(x)}{dx^2} = 0 \quad in \quad x \in (0, 1) \tag{23}$$

$$q(0) = 0 \quad q(1) = 1 \quad on \quad \partial\Omega. \tag{24}$$

Via the developed methodology, perturbed ODE (19) becomes

$$uQ_x - \varepsilon Q_{xx} - Q_{xx}\frac{h^2 u^2}{12\varepsilon} = 0, \tag{25}$$

indicating that only the second-order derivative perturbation term is required to achieve a higher order numerical solution in this case.

The computational stencil expression (8) reduces to

$$\begin{aligned} u(a_1 Q_{j-1} + a_2 Q_j + a_3 Q_{j+1}) - \varepsilon(a_4 Q_{j-1} + a_5 Q_j + a_6 Q_{j+1}) \\ - \frac{h^2 u^2}{12\varepsilon}(a_4 Q_{j-1} + a_5 Q_j + a_6 Q_{j+1}) = 0, \end{aligned} \tag{26}$$

where coefficients a_i are given in (13). Collecting the terms, the three node stencil is

$$\begin{aligned} \left[-\frac{6h\varepsilon u + 12\varepsilon^2 + h^2 u^2}{12\varepsilon h^2}\right] Q_{j-1} + \left[\frac{12\varepsilon^2 + h^2 u^2}{6\varepsilon h^2}\right] Q_j \\ + \left[\frac{6h\varepsilon u - 12\varepsilon^2 - h^2 u^2}{12\varepsilon h^2}\right] Q_{j+1} = 0. \end{aligned} \tag{27}$$

With this linear case development now complete, one can proceed to the nonlinear Burger's equation case, $f(x, q) = q(x)$. The one-dimensional steady-state equation is now of the form

$$L(q(x)) = \varepsilon \frac{d^2 q(x)}{dx^2} - q \frac{dq(x)}{dx} = 0 \quad in \quad x \in (0, 1), \tag{28}$$

with boundary conditions

$$q(0) = 1 \quad q(1) = -1. \tag{29}$$

The perturbed ODE form remains (19), with $f(x, q)$ replaced by $q(x)$. Replacing continuous derivative expressions with their discrete counterparts via (12), the computational stencil (8) takes the homogeneous form

$$\begin{aligned} F_j = {} & Q_j \left(-\frac{Q_{j-1}}{2h} + \frac{Q_{j+1}}{2h} \right) - \varepsilon \left(\frac{Q_{j-1}}{h^2} - \frac{2Q_j}{h^2} + \frac{Q_{j+1}}{h^2} \right) \\ & - \frac{h^2 Q_j}{12\varepsilon} \left(-\frac{Q_{j-1}}{2h} + \frac{Q_{j+1}}{2h} \right)^2 - \frac{h^2 Q_j^2}{12\varepsilon} \left(\frac{Q_{j-1}}{h^2} - \frac{2Q_j}{h^2} + \frac{Q_{j+1}}{h^2} \right) \\ & + \frac{h^2}{4} \left(-\frac{Q_{j-1}}{2h} + \frac{Q_{j+1}}{2h} \right) \left(\frac{Q_{j-1}}{h^2} - \frac{2Q_j}{h^2} + \frac{Q_{j+1}}{h^2} \right) = 0. \end{aligned} \tag{30}$$

The nonlinear system of equations (30) is solved using Newton's iterative procedure, with tridiagonal Jacobian matrix $\{JAC_{j-1}, JAC_j, JAC_{j+1}\}$ evaluated from (30) as

$$\begin{aligned} JAC_{j-1} = \frac{\partial F_j}{\partial Q_{j-1}} = {} & -\frac{1}{24\varepsilon h^2} \big(6Q_j \varepsilon h + 24\varepsilon^2 + h^2 Q_j Q_{j-1} \\ & - h^2 Q_j Q_{j+1} + 2Q_j^2 h^2 + 6Q_{j-1} \varepsilon h \big) \end{aligned} \tag{31}$$

$$\begin{aligned} JAC_j = \frac{\partial F_j}{\partial Q_j} = {} & -\frac{1}{48\varepsilon h^2} \big(12Q_{j-1} \varepsilon h - 12Q_{j+1} \varepsilon h - 96\varepsilon^2 \\ & + h^2 Q_{j-1}^2 - 2h^2 Q_{j-1} Q_{j+1} + h^2 Q_{j+1}^2 \\ & + 8h^2 Q_j Q_{j-1} - 24Q_j^2 h^2 + 8h^2 Q_j Q_{j+1} \big) \end{aligned} \tag{32}$$

$$\begin{aligned} JAC_{j+1} = \frac{\partial F_j}{\partial Q_{j+1}} = {} & \frac{1}{24\varepsilon h^2} \big(6Q_j \varepsilon h - 24\varepsilon^2 + h^2 Q_j Q_{j-1} \\ & - h^2 Q_j Q_{j+1} - 2Q_j^2 h^2 + 6Q_{j+1} \varepsilon h \big). \end{aligned} \tag{33}$$

TWO-DIMENSIONAL STEADY-STATE FORMULATION

Model equation (2) rewritten for the two-dimensional steady-state case and velocity $\mathbf{u}(\mathbf{x}, \mathbf{y}) = u(x, y)\mathbf{i} + v(x, y)\mathbf{j}$ becomes

$$\begin{aligned} L(q(x, y)) = {} & \varepsilon \frac{\partial^2 q(x, y)}{\partial x^2} + \varepsilon \frac{\partial^2 q(x, y)}{\partial y^2} - u(x, y) \frac{\partial q(x, y)}{\partial x} \\ & - v(x, y) \frac{\partial q(x, y)}{\partial y} = 0 \quad in \quad x, y \in (0, 1) \times (0, 1). \end{aligned} \tag{34}$$

In accordance with the Galerkin bilinear basis two-dimensional weak statement formulation written on rectangular four-node element, a fully discrete equivalent of (34), obtained

by assembling the element matrices on four adjacent elements sharing a common corner node, leads to the generic nine-node computational stencil

$$c_1 Q_{i-1,j-1} + c_2 Q_{i,j-1} + c_3 Q_{i+1,j-1} + c_4 Q_{i-1,j} + c_5 Q_{i,j} + c_6 Q_{i+1,j} + c_7 Q_{i-1,j+1} + c_8 Q_{i,j+1} + c_9 Q_{i+1,j+1} = 0. \tag{35}$$

Assuming a uniform square mesh with $\triangle x = \triangle y = h$, which is sufficiently small, and writing a Taylor series expansion at node i, j yields (36) with Q replacing $Q_{i,j}$ for clarity. Equation (36) represents an infinite order partial differential equation satisfied by the numerical solution. Retaining only the terms of the order lower or equal than four yields

$$\begin{aligned}
&(c_1 + c_2 + c_3 + c_4 + c_5 + c_6 + c_7 + c_8 + c_9) Q + h Q_x(-c_1 + c_3 - c_4 + c_6 - c_7 + c_9) \\
&+ h Q_y(-c1 - c_2 - c_3 + c_7 + c_8 + c_9) + \frac{h^2}{2} Q_{xx}(c_1 + c_3 + c_4 + c_6 + c_7 + c_9) \\
&+ \frac{h^2}{2} Q_{yy}(c_1 + c_2 + c_3 + c_7 + c_8 + c_9) + h^2 Q_{xy}(c_1 - c_3 - c_7 + c_9) \\
&+ \frac{h^3}{6} Q_{xxx}(c_9 - c_1 + c_3 - c_7 + c_6 - c_4) + \frac{h^3}{6} Q_{yyy}(c_9 - c_1 - c_3 + c_7 + c_8 - c_2) \\
&+ \frac{h^3}{2} Q_{xxy}(c_9 - c_1 - c_3 + c_7) + \frac{h^3}{2} Q_{xyy}(c_9 - c_1 + c_3 - c_7) \\
&+ \frac{h^4}{24} Q_{xxxx}(c_9 + c_1 + c_3 + c_7 + c_6 + c_4) + \frac{h^4}{24} Q_{yyyy}(c_9 + c_1 + c_3 + c_7 + c_8 + c_2) \\
&+ \frac{h^4}{6} Q_{xxxy}(c_9 + c_1 - c_3 - c_7) + \frac{h^4}{6} Q_{xyyy}(c_9 + c_1 - c_3 - c_7) \\
&+ \frac{h^4}{4} Q_{xxyy}(c_9 + c_1 + c_3 + c_7) + H.O.T. = 0.
\end{aligned} \tag{36}$$

As shown by Kolesnikov and Baker [21], the necessary symmetrization of the selected discretization is achieved via

$$\begin{aligned}
\sum_{n=1}^{9} c_n &= 0 \\
-c_1 + c_3 - c_4 + c_6 - c_7 + c_9 &= \frac{u}{h} \\
-c_1 - c_2 - c_3 + c_7 + c_8 + c_9 &= \frac{v}{h} \\
c_1 + c_3 + c_4 + c_6 + c_7 + c_9 &= -\frac{2\varepsilon}{h^2} \\
c_1 + c_2 + c_3 + c_7 + c_8 + c_9 &= -\frac{2\varepsilon}{h^2} \\
c_1 - c_3 - c_7 + c_9 &= 0 \\
c_9 - c_1 &= \frac{u+v}{6h} \\
c_9 + c_1 &= \frac{-\varepsilon}{3h^2} \\
c_3 - c_7 &= \frac{u-v}{6h},
\end{aligned} \tag{37}$$

which reduces (36) to

$$uQ_x + vQ_y - \varepsilon Q_{xx} - \varepsilon Q_{yy} + h^2\left(\frac{vQ_{yyy}}{6} + \frac{uQ_{xxx}}{6} + \frac{vQ_{xxy}}{6} + \frac{uQ_{xyy}}{6}\right) - h^2\varepsilon\left(\frac{Q_{xxxx}}{12} + \frac{Q_{yyyy}}{12} + \frac{Q_{xxyy}}{6}\right) + H.O.T. = 0. \quad (38)$$

In concert with the theoretical developments of the previous chapters, one can now differentiate (38) twice with respect to x and y and neglecting higher order terms obtain

$$u_{xx}Q_x + 2u_xQ_{xx} + uQ_{xxx} + v_{xx}Q_y + 2v_xQ_{xy} + vQ_{xxy} = \varepsilon Q_{xxxx} + \varepsilon Q_{xxyy} \quad (39)$$

$$u_{yy}Q_x + 2u_yQ_{xy} + uQ_{xyy} + v_{yy}Q_y + 2v_yQ_{yy} + vQ_{yyy} = \varepsilon Q_{xxyy} + \varepsilon Q_{yyyy}. \quad (40)$$

Similarly, differentiating (38) with respect to x and y produces

$$u_xQ_x + uQ_{xx} + v_xQ_y + vQ_{xy} = \varepsilon Q_{xxx} + \varepsilon Q_{xyy} \quad (41)$$

$$u_yQ_x + uQ_{xy} + v_yQ_y + vQ_{yy} = \varepsilon Q_{xxy} + \varepsilon Q_{yyy}. \quad (42)$$

Substituting expressions (39–42) into (36) leads to

$$uQ_x + vQ_y - \varepsilon Q_{xx} - \varepsilon Q_{yy} + h^2\left(\frac{vu_yQ_x}{12\varepsilon} + \frac{vuQ_{xy}}{6\varepsilon} + \frac{vv_yQ_y}{12\varepsilon} + \frac{v^2Q_{yy}}{12\varepsilon}\right) + h^2\left(\frac{uu_xQ_x}{12\varepsilon} + \frac{u^2Q_{xx}}{12\varepsilon} + \frac{uv_xQ_y}{12\varepsilon} - \frac{u_{xx}Q_x}{12} - \frac{u_xQ_{xx}}{6}\right) + h^2\left(-\frac{v_{xx}Q_y}{12} - \frac{v_xQ_{xy}}{6} - \frac{u_{yy}Q_x}{12} - \frac{u_yQ_{xy}}{6} - \frac{v_{yy}Q_y}{12} - \frac{v_yQ_{yy}}{6}\right) = 0, \quad (43)$$

which after reversing the sign on the truncation error terms yields the modified fourth-order perturbed PDE in the form

$$uQ_x + vQ_y - \varepsilon Q_{xx} - \varepsilon Q_{yy} - h^2\left(\frac{vu_yQ_x}{12\varepsilon} + \frac{vuQ_{xy}}{6\varepsilon} + \frac{vv_yQ_y}{12\varepsilon} + \frac{v^2Q_{yy}}{12\varepsilon}\right) - h^2\left(\frac{uu_xQ_x}{12\varepsilon} + \frac{u^2Q_{xx}}{12\varepsilon} + \frac{uv_xQ_y}{12\varepsilon} - \frac{u_{xx}Q_x}{12} - \frac{u_xQ_{xx}}{6}\right) - h^2\left(-\frac{v_{xx}Q_y}{12} - \frac{v_xQ_{xy}}{6} - \frac{u_{yy}Q_x}{12} - \frac{u_yQ_{xy}}{6} - \frac{v_{yy}Q_y}{12} - \frac{v_yQ_{yy}}{6}\right) = 0. \quad (44)$$

Again, note that for practical applications with smooth data and solution distributions, the $1/\varepsilon$ terms dominate. Hence, neglecting high-order correction terms of the order of 1, the remaining terms can be combined. The perturbed PDE (44) is then conveniently recast in continuum vector-form

$$\mathbf{u}\cdot\nabla q - \varepsilon\nabla\cdot\nabla q - \frac{h^2}{12\varepsilon}\mathbf{u}\cdot\nabla(\mathbf{u}\cdot\nabla q) = 0. \quad (45)$$

As before, discretization of perturbed equation (44) (consistent with (37)) will yield a fourth-order method because of the developed cancellation of the error terms. The partial

derivatives of the order h^2 present in (44) can be discretized via any conventional second-order FD/FV/FE method, since the error terms in their respective approximate expressions on a uniform mesh will be of the order h^4. The following are used in this development:

$$Q_x = -\frac{1}{2h}Q_{i-1,j} + \frac{1}{2h}Q_{i+1,j} \tag{46}$$

$$Q_y = -\frac{1}{2h}Q_{i,j-1} + \frac{1}{2h}Q_{i,j+1} \tag{47}$$

$$Q_{xy} = \frac{1}{4h^2}Q_{i-1,j-1} - \frac{1}{4h^2}Q_{i+1,j-1} - \frac{1}{4h^2}Q_{i-1,j+1} + \frac{1}{4h^2}Q_{i+1,j+1} \tag{48}$$

$$Q_{xx} = \frac{1}{h^2}Q_{i-1,j} - \frac{2}{h^2}Q_{i,j} + \frac{1}{h^2}Q_{i+1,j} \tag{49}$$

$$Q_{yy} = \frac{1}{h^2}Q_{i,j-1} - \frac{2}{h^2}Q_{i,j} + \frac{1}{h^2}Q_{i,j+1}. \tag{50}$$

Indeed, all approximations satisfy the matrix bandwidth restriction requirement and some may be easily recognized as their one-dimensional counterparts. While the approximation selection in (46–50) does not compromise the fourth-order accuracy of the method, the algorithm performance can be further optimized by customizing these discrete expressions.

The theoretical approach developed herein for the advection–diffusion example problems is directly applicable to the incompressible Navier–Stokes equation class as illustrated in the next section. Theory extension for the inviscid Euler equations is detailed in [20].

INCOMPRESSIBLE NAVIER–STOKES EQUATIONS: $\Omega - \Psi$ ALGORITHM

Navier–Stokes equation set governing two-dimensional flow of viscous incompressible fluid is written as (see, for example, [3])

$$\frac{\partial u_j}{\partial x_j} = 0 \tag{51}$$

$$\frac{\partial u_i}{\partial t} + \frac{\partial}{\partial x_j}\left(u_i u_j + \frac{p}{\rho_0}\delta_{ij} - \sigma_{ij}\right) + \frac{b_i}{Fr} = 0, \tag{52}$$

where ρ_0 is the constant density, u_j is the two-dimensional velocity vector, b_i is the body force, p is pressure, σ_{ij} is the Stokes stress tensor defined as

$$\sigma_{ij} = \frac{\nu}{Re}\left(\frac{\partial u_i}{\partial x_j} + \frac{\partial u_j}{\partial x_i}\right), \tag{53}$$

and nondimensional groups are defined as

$$Re = \frac{U_\infty L}{\nu_\infty} \tag{54}$$

$$Fr = \frac{U_\infty^2}{Lg}. \tag{55}$$

The constant density restriction allows for introduction of the streamfunction–vorticity variable set ψ, ω via

$$\mathbf{u} \equiv \nabla \times \psi \mathbf{k} \tag{56}$$

$$\omega \equiv \nabla \times \mathbf{u} \cdot \mathbf{k}, \tag{57}$$

which recasts the original system into

$$\frac{\partial \omega}{\partial t} + (\nabla \times \psi \mathbf{k} \cdot \nabla)\omega - \frac{1}{Re} \nabla^2 \omega = 0 \tag{58}$$

$$\nabla^2 \psi + \omega = 0, \tag{59}$$

with pressure being determined as a postprocessing operation via

$$\frac{1}{\rho_0} \nabla^2 p - \omega^2 + \frac{\partial^2 \psi}{\partial x^2} + \frac{\partial^2 \psi}{\partial y^2} + 2\frac{\partial^2 \psi}{\partial x \partial y} = 0. \tag{60}$$

Neglecting the body force contribution, writing (58, 59) in a component form and remembering definitions (56, 57) yields the Navier–Stokes system in the form

$$\frac{\partial \omega}{\partial t} + u\frac{\partial \omega}{\partial x} + v\frac{\partial \omega}{\partial y} - \frac{1}{Re}\frac{\partial^2 \omega}{\partial x^2} - \frac{1}{Re}\frac{\partial^2 \omega}{\partial y^2} = 0 \tag{61}$$

$$\frac{\partial^2 \psi}{\partial x^2} + \frac{\partial^2 \psi}{\partial y^2} + \omega = 0 \tag{62}$$

$$u = \frac{\partial \psi}{\partial y} \tag{63}$$

$$v = \frac{\partial \psi}{\partial x}. \tag{64}$$

Equation (61) is recognized as the unsteady advection–diffusion equation. Completion of the high-order formulation for this problem class therefore rests on the corresponding development for the stream-function Poisson equation. Assuming existence of the appropriate boundary conditions, generality of the developed theory readily provides a required extension. Here, one proceeds along a well-established design sequence.

Spatial discretization of (62) on a nine-node computational stencil results in

$$\begin{aligned} &W_{ij} + c_1\Psi_{i-1,j-1} + c_2\Psi_{i,j-1} + c_3\Psi_{i+1,j-1} + c_4\Psi_{i-1,j} + c_5\Psi_{i,j} \\ &+ c_6\Psi_{i+1,j} + c_7\Psi_{i-1,j+1} + c_8\Psi_{i,j+1} + c_9\Psi_{i+1,j+1} = 0. \end{aligned} \tag{65}$$

The approximation requirement as dictated by (36) and Taylor series expansion of (65) is

$$\sum_{n=1}^{9} c_n = 0$$

$$-c_1 + c_3 - c_4 + c_6 - c_7 + c_9 = 0$$

$$-c_1 - c_2 - c_3 + c_7 + c_8 + c_9 = 0$$

$$
\begin{aligned}
c_1 + c_3 + c_4 + c_6 + c_7 + c_9 &= \frac{2}{h^2} \\
c_1 + c_2 + c_3 + c_7 + c_8 + c_9 &= \frac{2}{h^2} \\
c_1 - c_3 - c_7 + c_9 &= 0 \\
c_9 - c_1 &= 0 \\
c_9 + c_1 &= \frac{1}{3h^2} \\
c_3 - c_7 &= 0,
\end{aligned}
\tag{66}
$$

which results in

$$
c_1 = \frac{1}{6h^2}, \quad c_2 = \frac{2}{3h^2}, \quad c_3 = \frac{1}{6h^2}, \quad c_4 = \frac{2}{3h^2}, \quad c_5 = -\frac{10}{3h^2} \tag{67}
$$

$$
c_6 = \frac{2}{3h^2}, \quad c_7 = \frac{1}{6h^2}, \quad c_8 = \frac{2}{3h^2}, \quad c_9 = \frac{1}{6h^2}, \tag{68}
$$

and reduces the corresponding truncation error expression to

$$
\omega + \psi_{xx} + \psi_{yy} + \frac{h^2}{12}\psi_{xxxx} + \frac{h^2}{12}\psi_{yyyy} + \frac{h^2}{6}\psi_{xxyy} + H.O.T. = 0. \tag{69}
$$

Differentiating (69) by xx and yy, neglecting high-order terms, and taking the linear combination of the resulting expressions, yields

$$
\psi_{xxxx} + 2\psi_{xxyy} + \psi_{yyyy} = -\omega_{xx} - \omega_{yy}. \tag{70}
$$

Substituting (70) into (69) and reversing the error term signs provides the desired fourth-order accurate perturbed PDE in the form

$$
\omega + \frac{\partial^2 \psi}{\partial x^2} + \frac{\partial^2 \psi}{\partial y^2} + \frac{h^2}{12}\left(\frac{\partial^2 \omega}{\partial x^2} + \frac{\partial^2 \omega}{\partial y^2}\right) = 0. \tag{71}
$$

The modified continuous system composed of four coupled equations written for four variables ω, ψ, u, v now is

$$
\frac{\partial \omega}{\partial t} + \mathbf{u} \cdot \nabla \omega - \frac{1}{Re}\nabla \cdot \nabla \omega - \frac{h^2 Re}{12}\mathbf{u} \cdot \nabla(\mathbf{u} \cdot \nabla \omega) = 0 \tag{72}
$$

$$
\omega + \nabla \cdot \nabla \psi + \frac{h^2}{12}\nabla \cdot \nabla \omega = 0 \tag{73}
$$

$$
u = \frac{\partial \psi}{\partial y} \tag{74}
$$

$$
v = \frac{\partial \psi}{\partial x}, \tag{75}
$$

with pressure being determined via (60) as a postprocessing operation.

Note that the selected formulation for the corrected vorticity equation (72) is consistent with the continuum vector form (44). One therefore cannot expect the numerical solution

to attain the design fourth-order of accuracy. Nevertheless, computational results show the remaining correction terms to retain the desirable stabilizing effects of the high-order formulation.

RESULTS AND DISCUSSION

Asymptotic Convergence Estimates

Since an analytical solution is not generally available, the following analysis [3] is used to confirm the predicted convergence rate of the developed methods. For the lead term of the truncation series expansion given in the form

$$error^h \simeq C_k h_e^{2k} \tag{76}$$

and using

$$T^h + e^h = T_{exact} = T^{h/2} + e^{h/2}, \tag{77}$$

one can easily verify that

$$e^h = (2^{2k}) e^{h/2} \tag{78}$$

and therefore

$$T^{h/2} - T^h = (2^{2k} - 1) e^{h/2}, \quad e^{h/2} = \frac{\triangle T^{h/2}}{2^{2k} - 1}. \tag{79}$$

Here $\triangle T^{h/2} = T^{h/2} - T^h$ denotes the computed difference in the two approximate solutions. Selecting a *log* representation, the slope of the convergence curve should be

$$slope = \frac{log\left(e^{h/M}\right) - log\left(e^{h/2M}\right)}{log(h) - log(h/2)} = \frac{log\left(e^{h/M}/e^{h/2M}\right)}{log(2)}, \tag{80}$$

where M is the number of finite elements used in computing the solution.

One-Dimensional Advection–Diffusion

Convergence data computed for the derived methods are presented in the Tables I and II. Table I lists data obtained for the scalar case (23) and Table II for the nonlinear case (28). All data were computed for $\varepsilon = 0.1$.

Computed slope values confirm Taylor series-predicted convergence rates of the developed methods. When compared to the exact solution $Q(x = 0.75) = 0.0820433$ in the scalar case ($\varepsilon = 0.1$), the fourth-order method evidences superior performance. Specifically, monotone and accurate results are obtained on a relatively coarse mesh. A tenfold mesh refinement would be required for the second-order method to produce comparable results. This seemingly insignificant "third digit" observation will become extremely important in costly real-life computations.

Solution evolution for the linear advection–diffusion for $\varepsilon = 0.001$ is shown in Fig. 1 with number of nodes *Nnode*. Presented are numerical solutions computed using fourth-order

TABLE I
Perturbed PDE Method. 1D Linear Advection–Diffusion, $\varepsilon = 0.1$

Nnode	Q(x = 0.75)	△Q	Slope
	(a) Fourth-order method		
9	0.08280510	—	—
17	0.08208770	0.0007174	—
33	0.08204605	0.00004165	4.107
65	0.0820434	0.00000255	4.03
129	0.08204337	0.00000012	4.41
	(b) Second-order method		
9	0.05324680	—	—
17	0.07525270	0.02200590	—
33	0.08036900	0.00511630	2.105
65	0.08162610	0.00125700	2.025
129	0.081193910	0.00313000	2.006

and second-order methods. Even for this modest value of ε, Galerkin linear basis solution remains oscillatory in the boundary region for all considered discretizations. The well-known monotonicity constraint [11, 28] applied to $\varepsilon = 0.001$ states that at least 500 nodes are needed for Galerkin linear basis discretization to produce a nonoscillatory (monotone) solution.

In contrast, the fourth-order method solutions remain monotone independent of *Nnode*, albeit overdiffused on the coarse ($Nnode = 21$) mesh, in full agreement with high-order method results reported by Fletcher [11]. While the coarse mesh solution is clearly overdiffused, a reasonable 121-node discretization of the solution domain allows for the computing of an acceptable solution. Further refinement results in a highly accurate monotone solution for $Nnode = 221$.

Results computed for the Burger's equation case are shown in Fig. 2 for $\varepsilon = 0.001$. The fourth-order accurate solutions are presented for various discretizations. Presented solutions

TABLE II
Perturbed PDE Method. 1D Burger's Equation, $\varepsilon = 0.1$

Nnode	Q(x = 0.25)	△Q	Slope
	(a) Fourth-order method		
9	0.85629180	—	—
17	0.86320770	0.00691590	—
33	0.86351750	0.00030980	4.48
65	0.86353430	0.00001680	4.205
129	0.86353536	0.00000106	3.987
	(b) Second-order method		
9	0.90590460	—	—
17	0.87307980	0.03282480	—
33	0.86586460	0.00721520	2.185
65	0.86411420	0.00175040	2.044
129	0.86368005	0.00043415	2.012

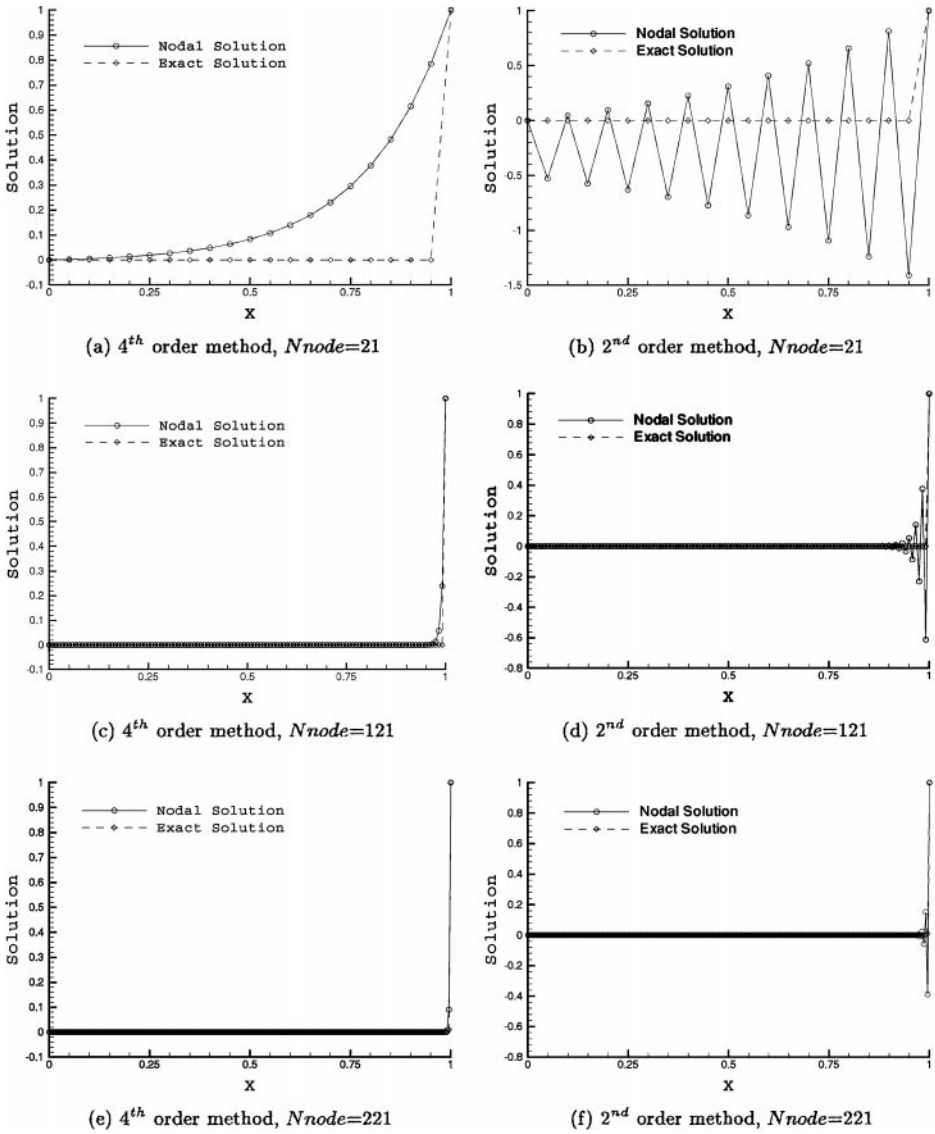

FIG. 1. Linear advection–diffusion, solution dependence on *Nnode*, $\varepsilon = 0.001$. High-order and GWS performance comparison.

follow general trends observed for the linear case, highlighting continuity of the developed theoretical approach. All solutions are monotone with highly accurate results obtained on sufficiently refined discretizations. The second-order method solution (not shown here) was divergent. In fact, continuing the iteration process (up to 50 iterations, not shown) does not improve the solution, but rather exaggerates its divergent behavior.

Overall, computational results illustrate two main points. Namely, high-order methods can achieve desirable error levels on coarser meshes, and for a given mesh, high-order methods produce more accurate results. The developed theoretical approach allows for exercising these advantages at no added computational cost, which is usually associated with solution matrix bandwidth expansion of high-order accurate methods.

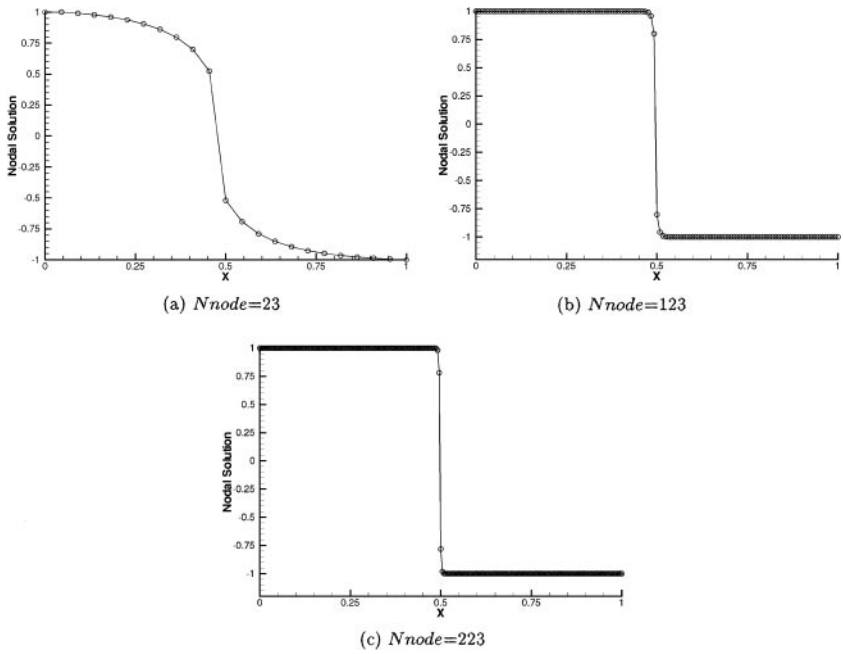

FIG. 2. Burgers equation. Fourth-order method solutions on uniform mesh, $\varepsilon = 0.001$.

Two-Dimensional Advection–Diffusion

Uniform mesh refinement results confirming predicted convergence rates of the developed fourth-order method are shown in Table III.

All data were computed at the center node of the solution domain $x = 0.5$, $y = 0.5$. For the purpose of establishing the convergence rate of the method, the linear problem with the exact boundary conditions

$$q(1, 1) = 1 \quad q(0, y) = q(x, 0) = 0 \tag{81}$$

TABLE III
Perturbed PDE Method. 2D Linear Advection–Diffusion. Fourth-Order Convergence Data

(a) $\varepsilon = 1$			
Nnode	Q	$\triangle$Q	Slope
3×3	0.14254288	—	—
5×5	0.14253726	0.000005626	—
9×9	0.14253697	0.000000287	4.29
17×17	0.14253695	0.000000017	4.08
(b) $\varepsilon = 0.1$			
Nnode	$Q \times 10^{-5}$	$\Delta Q \times 10^{-5}$	Slope
9×9	0.468156	—	—
17×17	0.448714	0.01944	—
33×33	0.447985	0.00073	4.74
65×65	0.447945	0.00004	4.19

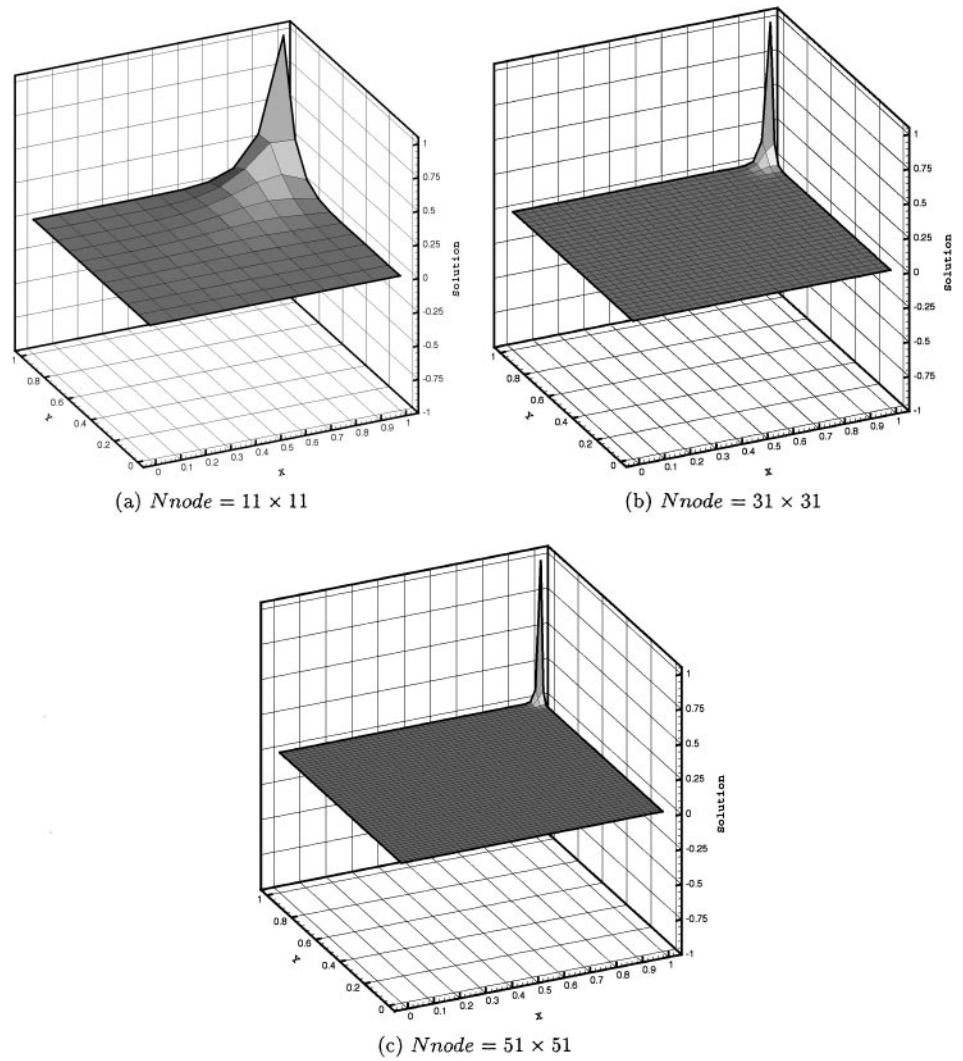

(a) $Nnode = 11 \times 11$ (b) $Nnode = 31 \times 31$

(c) $Nnode = 51 \times 51$

FIG. 3. Linear advection–diffusion, uniform mesh, solution dependence on *Nnode*, $\varepsilon = 0.005$.

$$q(x,1) = \frac{e^{\frac{ux}{\varepsilon}} - 1}{e^{\frac{1}{\varepsilon}} - 1} \quad q(1,y) = \frac{e^{\frac{vy}{\varepsilon}} - 1}{e^{\frac{1}{\varepsilon}} - 1} \tag{82}$$

were considered in the mesh refinement study.

Numerical results in Fig. 3 present solutions to the linear problem computed on several uniform discretizations for $\varepsilon = 0.005$. The boundary conditions (82) were replaced with the adiabatic conditions

$$\frac{\partial q(x,1)}{\partial \mathbf{n}} = \frac{\partial q(1,y)}{\partial \mathbf{n}} = 0. \tag{83}$$

The fourth-order method yields monotone results on all discretizations. An inaccurate, overdiffused solution on a coarse 11×11 grid is significantly improved after a modest mesh refinement (Fig. 3b). Further mesh refinement produces an excellent solution on a 51×51 node mesh.

Driven-Cavity Benchmark Solutions

The driven-cavity problem is a well-known validation benchmark problem [3, 7, 30, 37]. The solution domain is the unit square, with the lid defined to slide across the domain at a uniform velocity.

The high-order formulation developed for the incompressible Navier–Stokes vorticity–streamfunction formulation was shown to incorporate the fundamentals of the classic TWS analysis. The correction error terms necessary for the appropriate order of accuracy are combined via vector analysis to provide the β term of the TWS formulation. The theoretical analysis results in a highly efficient dispersion error control mechanism whose application is based on the specifics of the solution domain discretization and physics of the problem. It is this theoretically sound control mechanism that distinguishes this development, allowing for selective application of optimal amounts of diffusion for maximum accuracy as dictated by the high-order accuracy formulation. It is important to note that unlike the TWS formulation, present development also includes the reformulated Poisson streamfunction equation as an integral part of a high-order accurate solution process.

Numerical results for a range of Reynolds numbers are shown in Figs. 4 and 5. Compared are GWS, TWS, and newly developed high-order method formulations. For a modest value of $\mathrm{Re} = 1000$ all solutions are of reasonable engineering quality, with GWS vorticity solution showing some oscillatory behavior. Oscillations are significantly reduced via the TWS β-term application and are nonexistent on the fourth-order method solution.

The picture changes significantly as the Reynolds number is increased to 3000. As shown in Fig. 5, GWS and TWS solutions are unacceptably polluted by oscillations, with high-order formulation providing a excellent monotone solution on a rather coarse locally uniform mesh. This locally uniform discretization is quantized via the *a*PSE notation as X1: [33(0. 8R1.0 .02 16R1.0 .98 8R1.0 1)] and X2: [−33(0. 20R1.0 .98 12R1.0 1)], which reads for X1: "from 0 to 0.02 place 8 nodes with the progression ratio of 1.0 (uniformly), from 0.02 to 0.98 uniformly place 16 nodes and finally from 0.98 to 1.0 uniformly place 8 nodes." Similarly, notation for X2 reads: "from 0 to 0.98 uniformly place 20 nodes, from 0.98 to 1.0 uniformly place 12 nodes."

The numerical results illustrate a definite advantage of theoretically predicted selective application of numerical diffusion provided by the error correction terms over the entire solution domain. Note that packing more nodes at the boundaries of the solution domain would result in monotone solutions for both GWS and TWS formulations. Of course, the price one pays is the information lost on the interior of the solution domain with the discretization nodes migrating to the boundaries.

The importance of considering a high-order formulation consisting of the perturbed PDEs for both vorticity and streamfunction equations in illustrated in Figs. 6–8. Figures 6 and 7 show the results obtained when the high-order formulation is only used for the vorticity equation while the streamfunction equation remains (59). The solution is comparable to that of the TWS method in Fig. 5. In contrast, Fig. 8 shows the solution computed when only the streamfunction equation is modified with vorticity being calculated via the original equation. One may conclude that for this particular problem class, high-order modification of the streamfunction equation is more significant as compared to that of the vorticity equation, but both are required for a consistent high-order formulation.

Results from the uniform mesh convergence study conducted for stream-function variable in energy norm using both GWS and high-order formulation with $\mathrm{Re} = 10$ and $\mathrm{Re} = 100$ are

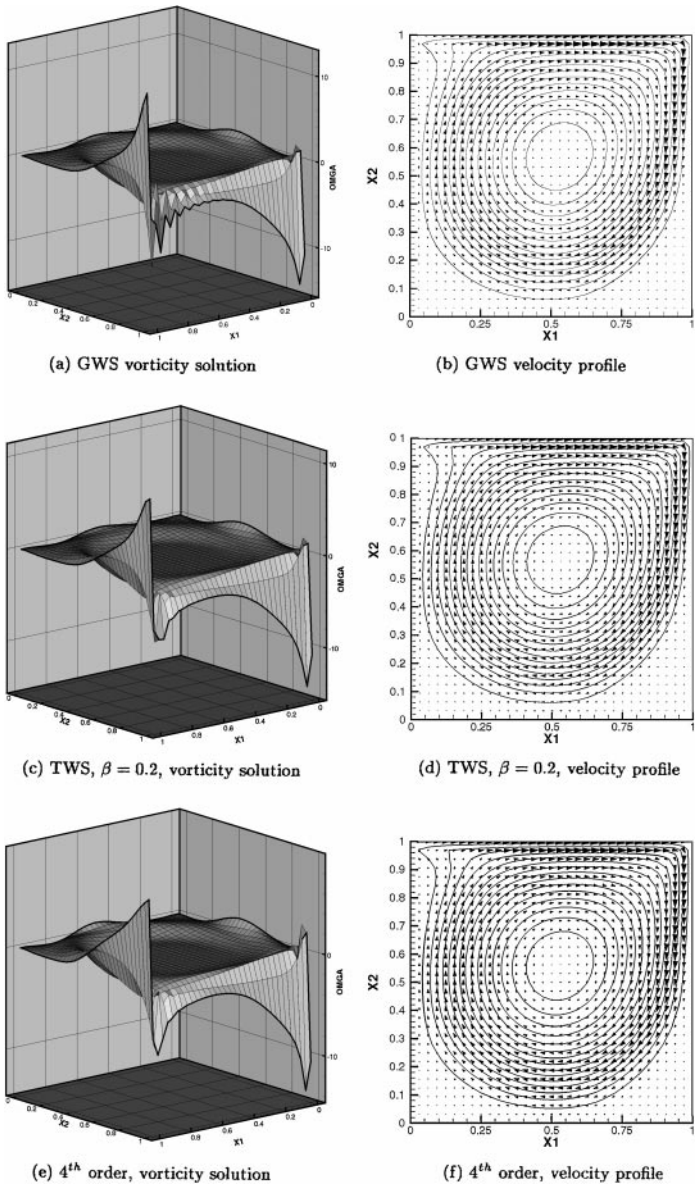

FIG. 4. Driven-cavity benchmark solutions. Re = 1000, 33 × 33 node uniform mesh.

shown in Table IV. All solutions were time-iterated to steady-state. Obtained convergence data indicate near-second-order convergence for both methods, reflecting time-integration second-order of accuracy. While the nominal order of accuracy in the high-order formulation is reduced, the desirable performance trend of the high-order method is nevertheless preserved. This is seen from the convergence data obtained for Re = 100 on coarser (9×9 and 17×17) discretizations. Consistent with the results reported for the model advection–diffusion problem, high-order formulation achieves monotone solutions on coarser meshes, resulting in higher convergence rates and more accurate numerical results. The convergence data computed for the high-order formulation illustrates the relative importance of the terms neglected in designing the continuous vector form of the perturbed PDE in (45). These terms

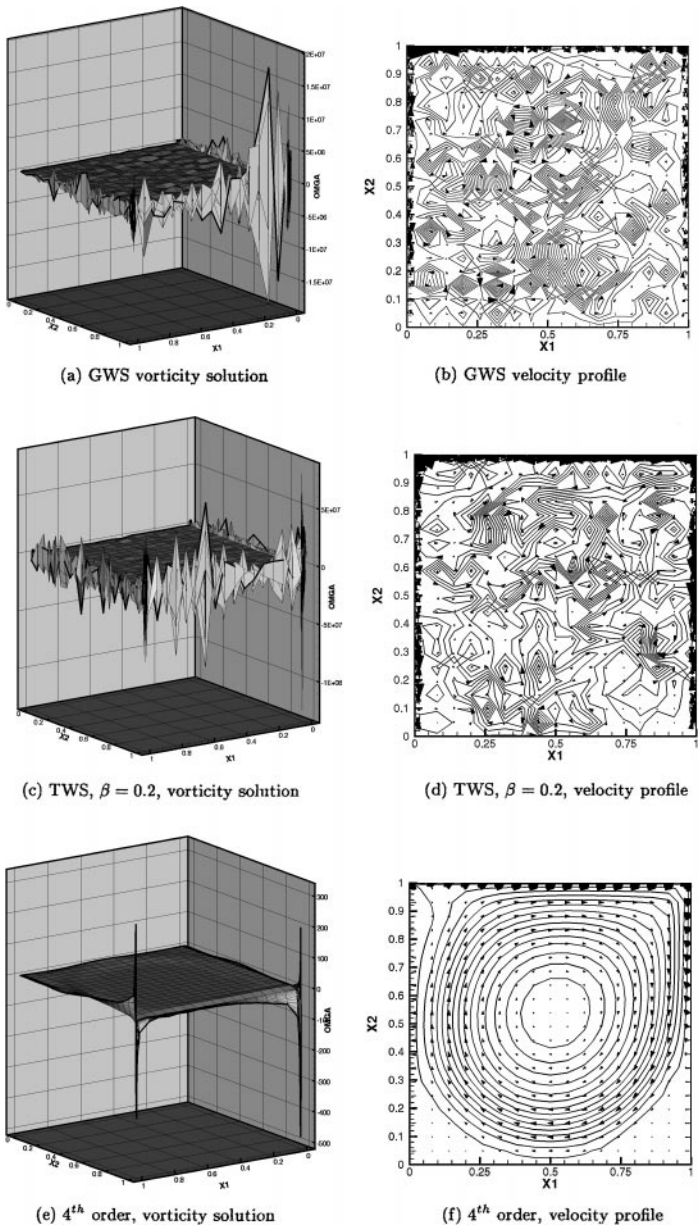

FIG. 5. Driven-cavity benchmark solutions. Re = 3000, 33 × 33 node locally uniform mesh. X1: [33(0. 8R1.0 .02 16R1.0 .98 8R1.0 1)], X2: [33(0. 20R1.0 .98 12R1.0 1)].

are of greater significance when dealing with low Reynolds number flows, resulting in lower convergence rates. When the Reynolds number increases, the convergence rate improves because of the diminished contribution from the neglected terms.

The accuracy of the GWS, TWS, and high-order formulations was tested by comparing their respective numerical solutions to fine-mesh benchmark results established on a 256 × 256 mesh by Ghia *et al*. [12]. Table V summarizes driven-cavity benchmark data comparisons. For the purpose of obtaining near-monotone solutions for all considered methods, uniform 33 × 33 node discretization was used for Re = 100, 400, 1000, while the

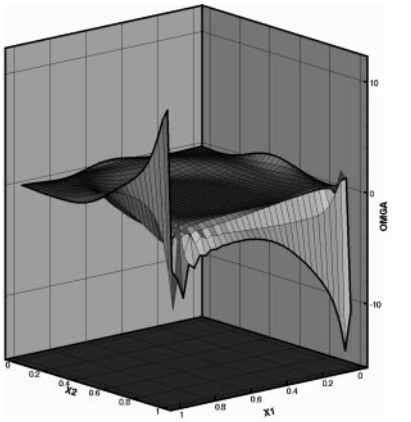

(a) Vorticity solution, Re=1000

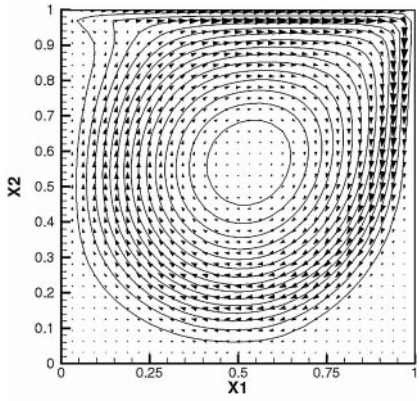

(b) Velocity profile, Re=1000

FIG. 6. Driven-cavity benchmark solutions. Vorticity high-order formulation. 33 × 33-node uniform mesh.

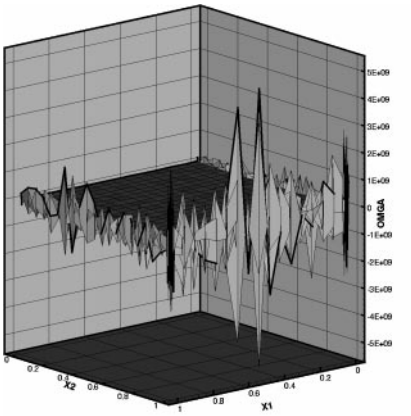

(a) Vorticity solution, Re=3000

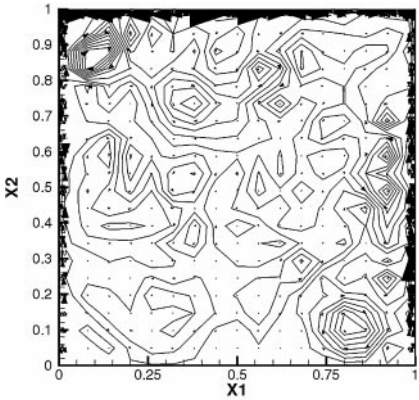

(b) Velocity profile, Re=3000

FIG. 7. Driven-cavity benchmark solutions. Vorticity high-order formulation. 33 × 33-node locally uniform mesh. X1: [33(0. 8R1.0 .02 16R1.0 .98 8R1.0 1)], X2: [−33(0. 20R1.0 .98 12R1.0 1)].

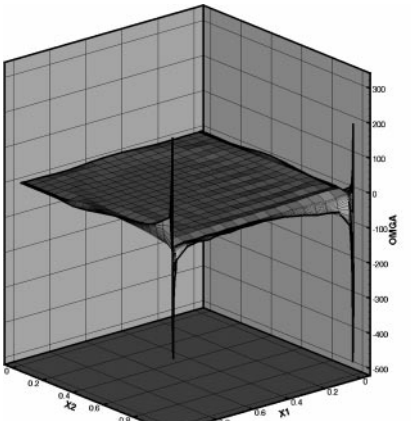

(a) Vorticity solution, Re=3000

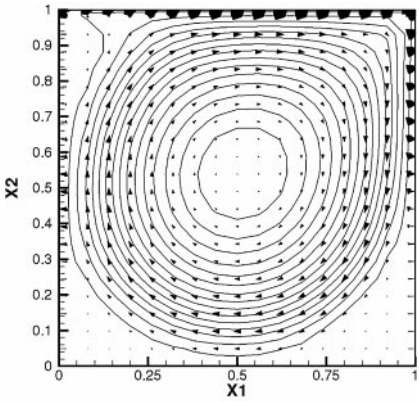

(b) Velocity profile, Re=3000

FIG. 8. Driven-cavity benchmark solutions. Streamfunction high-order formulation. 33 × 33-node locally uniform mesh. X1: [33(0. 8R1.0 .02 16R1.0 .98 8R1.0 1)], X2: [−33(0. 20R1.0 .98 12R1.0 1)].

TABLE IV
Driven-Cavity Benchmark Convergence Study.
Streamfunction in Energy Norm

Nnode	$\|\Psi\| \times 10^{-2}$	$\|\triangle\Psi\| \times 10^{-2}$	Slope
	(a) Re = 10, high-order formulation		
9×9	2.8577	—	—
17×17	3.2011	0.3434	—
33×33	3.3113	0.1102	1.64
65×65	3.3443	0.0330	1.74
	(b) Re = 10, GWS formulation		
9×9	2.8535	—	—
17×17	3.1998	0.3463	—
33×33	3.3110	0.1112	1.64
65×65	3.3442	0.0332	1.74
	(c) Re = 100, high-order formulation		
9×9	3.1670	—	—
17×17	3.4033	0.2363	—
33×33	3.4364	0.0331	2.84
65×65	3.4422	0.0058	2.51
	(d) Re = 100, GWS formulation		
9×9	2.7706	—	—
17×17	3.2747	0.5041	—
33×33	3.4023	0.1276	1.98
65×65	3.4332	0.0309	2.05

locally uniform discretization quantized as X1: [33(0. 9R1.0 .02 14R1.0 .98 9R1.0 1)], X2: [−33(0.18R1.0 .98 14R1.0 1)] was used for Re = 3200. The study compares the maximum values of the streamfunction variable achieved over the entire solution domain (ψ_{max}), together with the value of the vorticity variable computed at the same nodal location, as produced by the considered methods. For consistency, the TWS β parameter was set to 0.2 in all computations. High-order and GWS formulations yield similar results, with the high-order method being consistently more accurate. The TWS method results are overdiffused via the β parameter selection for Re = 100, 400 and produce accurate results for Re = 1000.

TABLE V
Driven-Cavity Benchmark Accuracy Comparison

Re	Ghia *et al.*	GWS	TWS $\beta = 0.2$	High-order
		(a) $\|\Psi\|_{max}$		
100	0.103423	0.10377	0.08745	0.10358
400	0.113909	0.11467	0.11067	0.11771
1000	0.117929	0.11881	0.12059	0.11835
3200	0.120377	0.11835	0.11831	0.11836
		(b) Vorticity ω		
100	3.16646	3.29898	3.08023	3.30388
400	2.29469	2.31917	2.31133	2.31648
1000	2.04908	2.09925	2.12341	2.10249
3200	1.98860	1.49245	1.88762	2.10410

Overall, the numerical results obtained for the driven-cavity benchmark problem confirm the advantages of using the developed high-order formulation. This formulation allows for achieving monotone accurate numerical solutions on coarser discretizations as compared to GWS and TWS methods. This preserves the high-order solution trends illustrated for the model advection–diffusion problem and provides for a better resolution of the interior of the solution domain. The application of the correction error terms developed herein is governed by physics of the problem and does not require many knobs and switches to run the problem.

CONCLUSIONS

A new approach to designing high-order accurate CFD methods has been developed and tested for a range of problem statements belonging to the incompressible Navier–Stokes equation system. The systematic construction of progressively higher order spatial approximations is achieved via a modified equation analysis, which allows one to determine the computational stencil coefficients appropriate to a desired accuracy order. The resulting high-order error correction terms are shown to be consistent with the β term characteristic of the TWS finite element formulation. This confirms the expected high-order of spatial accuracy in TWS constructions and provides a highly efficient dispersion error control mechanism, whose application is based on the specifics of the solution domain discretization and physics of the problem.

Theoretical development utilizes fundamentals of the finite element weak statement formulation and truncation error analysis to characterize error in the numerical solution process. It then offers a computationally inexpensive way of constructing equation-specific higher order approximations. A distinguishing desirable property of the developed method is solution matrix bandwidth, which always remains equal to that of the second-order discretization. This permits combining the computational efficiency of the lower order methods with superior accuracy inherent in high-order approximations. Generality of the underlying principles is shown to provide a natural transition of the concepts derived for the one-dimensional steady-state case to multidimensional and unsteady problems. The perturbed PDE analysis is further demonstrated to be widely applicable to Navier–Stokes nonlinear equation law system, with the theoretical development yielding the continuous vector forms needed for the appropriate error corrections.

Numerical simulations compare performance of the developed method to that of the GWS and TWS formulations. Uniform mesh refinement convergence results confirm the order of truncation error for each method. High-order formulation is shown to require significantly fewer nodes to accurately resolve solution gradients for convection dominated problems. Benchmark problem applications for the incompressible Navier–Stokes equations complete the manuscript. In both cases, the developed high-order formulation is shown to result in more accurate solutions on coarser discretizations, thus preserving the design trends illustrated for the model advection–diffusion equation. The theoretical development is therefore complete.

REFERENCES

1. C. Baiocchi, F. Brezzi, and L. P. Franca, Virtual bubbles and Galerkin-least-squares type methods, *Comp. Meth. Appl. Mech. Eng.* **105**, 125 (1993).

2. A. J. Baker and J. W. Kim, A Taylor weak-statement algorithm for hyperbolic conservation laws, *Int. J. Numer. Meth. Fluids* **7**, 489 (1987).
3. A. J. Baker, *Finite Element Computational Fluid Dynamics* (Hemisphere, New York, 1983).
4. A. J. Baker and D. W. Pepper, *Finite Elements 1-2-3* (McGraw-Hill, New York, 1991).
5. A. N. Brooks and T. J. R. Hughes, Streamline upwind Petrov–Galerkin methods for advection dominated flows, in *Proceedings Third International Conference on Finite Element Methods in Fluid Flow, Banff, 1980*.
6. D. J. Chaffin and A. J. Baker, On Taylor weak statement finite element methods for computational fluid dynamics, *Int. J. Numer. Meth. Fluids* **21**, 273 (1995).
7. D. J. Chaffin, *A Taylor Weak Statement Finite Element Method for Computational Fluid Dynamics*, Ph.D. dissertation (The University of Tennessee, Knoxville, 1997).
8. I. Christie and A. R. Mitchell, Upwinding of high order Galerkin methods in conduction–convection problems, *Int. J. Numer. Meth. Eng.* **12**, 1764 (1978).
9. L. Collatz, *The Numerical Treatment of Differential Equations* (Springer-Verlag, Berlin, 1960).
10. J. Donea, A Taylor–Galerkin method for convective transport problems, *Int. J. Numer. Meth. Eng.* **20**, 101 (1984).
11. C. A. J. Fletcher, *Computational Techniques for Fluid Dynamics 1: Fundamental and General Techniques* (Springer-Verlag, New York, 1991).
12. U. Ghia, K. N. Ghia, and C. T. Shin, High-Re solutions for incompressible flow using the Navier–Stokes equations and a multi-grid method, *J. Comput. Phys*. **48**, 387 (1982).
13. J. C. Heinrich, P. S. Huyakorn, O. C. Zienkiewicz, and A. R. Mitchell, An "upwind" finite element scheme for two-dimensional convective transport equation, *Int. J. Numer. Meth. Eng.* **11**, 131 (1977).
14. C. Hu and C.-W. Shu, *A Discontinuous Galerkin Finite Element Method for Hamilton–Jacobi Equations*, ICASE Report 98-2 (Jan. 1998).
15. C. Hu and C.-W. Shu, *Weighted Essentially Non-oscillatory Schemes on Triangular Meshes*, ICASE Report 98-32 (July 1998), available at http://www.icase.edu.
16. J. Iannelli, *NEWS: A Non-linear Element-Upstream Weak Statement for the Euler and Navier–Stokes Equations*, Technical Paper 96-0763 (AIAA Press, Washington, DC, 1996).
17. J. Iannelli, A CFD Euler solver from a physical acoustics-convection flux jacobian decomposition, *Int. J. Numer. Meth. Fluids* **31**, 821 (1999).
18. J. W. Kim and D. J. Lee, Optimized compact finite difference schemes with maximum resolution, *AIAA J.* **34**, 887 (1996).
19. J. W. Kim and D. J. Lee, Numerical simulation of nonlinear waves using optimized high-order compact schemes, *Comput. Fluids Dyn. J*. **5**, 281 (1996).
20. A. Kolesnikov, *Efficient Implementation of High Order Methods in Computational Fluid Dynamics*, Ph.D. dissertation (The University of Tennessee, Knoxville, 2000).
21. A. Kolesnikov and A. J. Baker, Efficient implementation of high order methods for the advection–diffusion equation, *Comput. Math. Appl. Mech. Eng*. **189**, 701 (2000).
22. Z. Kopal, *Numerical Analysis* (Wiley, New York, 1961).
23. P. Lax and B. Wendroff, Systems of conservation laws, *Commun. Pure Appl. Math*. **8**, 217 (1960).
24. B. P. Leonard, The ULTIMATE conservative difference scheme applied to unsteady one-dimensional advection, *Comput. Meth. Appl. Mech. Eng*. **88**, 17 (1991).
25. H. Lomax, Recent progress in numerical techniques for flow simulation, *AIAA J.* **14**, 512 (1976).
26. W. P. Noronha and A. J. Baker, A Taylor weak statement finite element CFD algorithm for 2D incompressible Navier Stokes equations, presented at the AIAA 27th Aerospace Sciences Meeting, Reno, Nevada, 1989.
27. J. T. Oden, Optimal h–p finite element methods, *Comput. Meth. Appl. Mech. Eng*. **112**, 309 (1994).
28. S. Roy and A. J. Baker, SGM-Part I, *Int. J. Numer. Heat Transfer* **31**, 135 (1997).
29. S. Roy and A. J. Baker, SGM-Part II, *Int. J. Numer. Heat Transfer, Part B* **33**, 5 (1998).
30. S. Roy, *On Improved Methods for Monotone CFD Solution Accuracy*, Ph.D. dissertation (The University of Tennessee, Knoxville, 1994).
31. Yu. I. Shokin, *The Method of Differential Approximation* (Springer-Verlag, Berlin/New York, 1983).

32. C.-W. Shu, Essentially non-oscillatory and weighted essentially non-oscillatory schemes for hyperbolic conservation laws, ICASE Report 97-65 (1997), available at http://www.icase.edu.
33. C. K. W. Tam and J. C. Webb, Dispersion-relation preserving finite difference schemes for computational acoustics, *J. Comput. Phys.* **107**, 262 (1993).
34. J. W. Thomas, *Numerical Partial Differential Equations* (Springer-Verlag, New York, 1995).
35. M. R. Visbal and D. V. Gaitonde, *High-Order Accurate Methods for Unsteady Vortical Flows on Curvilinear Meshes*, Technical Paper 98-0131 (AIAA Press, Washington, DC, 1998).
36. R. F. Warming and B. J. Hyett, The modified equation approach to the stability and accuracy analysis of finite difference methods, *J. Comput Phys.* **14**, 159 (1974).
37. P. Williams, *A Three-Dimensional, Time-Accurate, Incompressible, Navier Stokes Finite Element CFD Algorithm*, Ph.D. dissertation (The Unbiversity of Tennessee, Knoxville, 1993).